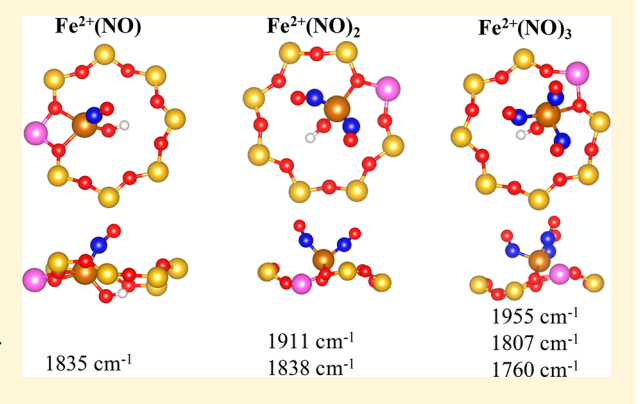


Modeling the Adsorption of NO and NH₃ on Fe-SSZ-13 from First-**Principles: A DFT Study**

Rengin Zhang, [†] Emily Anderst, [†] Kyle Groden, [†] and Jean-Sabin McEwen*, [†], [‡], [§], ||, [†]

Supporting Information

ABSTRACT: As emission standards continue to tighten, there is a critical need for more selective and efficient methods to remove NO_x from the exhaust of lean-burn engines. Currently, the predominant method employed for NO_x removal is through selective catalytic reduction (SCR) using ammonia as a reducing agent. Typically, Fe- and Cu-exchanged CHA catalysts (Fe-SSZ-13 and Cu-SSZ-13) are used, but much less is known about Fe-SSZ-13 as compared to Cu-SSZ-13, which has been extensively characterized via experimental and computational techniques. In this work, density functional theory (DFT) calculations were performed to determine the most likely adsorption complexes that form within the six- or eight-membered rings (6MR or 8MR) of Fe-SSZ-13. We examine both Fe²⁺ (as [Fe(OH)]⁺) and Fe³⁺ (as [Fe(OH)]²⁺) as the possible active sites. Based on our results, the



most energetically favorable site lies initially within the 6MR. However, with the addition of adsorbates, we find that the 8MR sites become more energetically favorable. Our results show, for an Fe²⁺ cation, that the most stable configuration occurs within the 8MR, where NO is coadsorbed on Fe with an OH ligand. For an Fe³⁺ cation, the lowest energy configuration occurs when NO adsorbs directly onto Fe within the 8MR without interacting with the OH ligand. The vibrational frequencies of chemisorbed NO were also calculated and compared with the experimental IR spectra. The experimental values for such frequencies agree well with the DFT-calculated values, except for Fe²⁺(NO)₂. We anticipate that this improved understanding of the structural and electronic features of Fe-SSZ-13 will be useful for the future determination of the underlying SCR reaction mechanism on Fe-SSZ-13.

1. INTRODUCTION

"Lean-burn" engines offer improved fuel economy as compared to engines operating with stoichiometric air-to-fuel ratios. However, this increased efficiency comes at a cost, as harmful nitrogen oxides (NO_x) are major pollutants in the exhaust from these engines.² As such, removing NO_x is a challenge in "lean-burn" engines.^{1,3} As is well-known, these species can be removed through selective catalytic reduction (SCR) with ammonia, which is a reaction between NO, NO2, and O2 oxidants and an NH₃ reductant to form N₂ and H₂O. Copperexchanged SSZ-13 (Cu-SSZ-13), which is a zeolite with the chabazite (CHA) structure, shows excellent activity and selectivity toward the formation of N₂ in the SCR of NO_x with NH₃. ^{4,5} This has prompted studies of Cu-SSZ-13 via both experimental and computational techniques to elucidate the fundamental chemistry that is responsible for both its activity and its selectivity. 4,6-20 Iron-exchanged zeolites (most notably

Fe-ZSM-5) have also been extensively studied as SCR catalysts for removing NO_x. ²¹ Recently, Fe-based exchanged CHA catalysts (Fe-SSZ-13) have started to receive a significant amount of attention. One of the first investigations on such materials was performed by Gao et al., who characterized and benchmarked their SCR performance.²² They concluded that Fe-SSZ-13 could be used as a co-catalyst with Cu-SSZ-13 for SCR after-treatment, based on its high temperature activity and stability after hydrothermal aging. They further concluded that NH₃ inhibition (which could be understood in two ways: (1) NH₃ binds with Fe centers strongly; and (2) Fe ions are trapped in the +2 oxidation state, because of the reduction by

August 1, 2018 Received: Revised: September 16, 2018 Accepted: September 17, 2018 Published: September 17, 2018

[†]The Gene and Linda Voiland School of Chemical Engineering and Bioengineering, Washington State University, Pullman, Washington 99164, United States

^{*}Department of Physics and Astronomy, Washington State University, Pullman, Washington 99164, United States

[§]Department of Chemistry, Washington State University, Pullman, Washington 99164, United States

Institute for Integrated Catalysis, Pacific Northwest National Laboratory, Richland, Washington 99352, United States

 $^{^\}perp$ Department of Biological Systems Engineering, Washington State University, Pullman, Washington 99164, United States

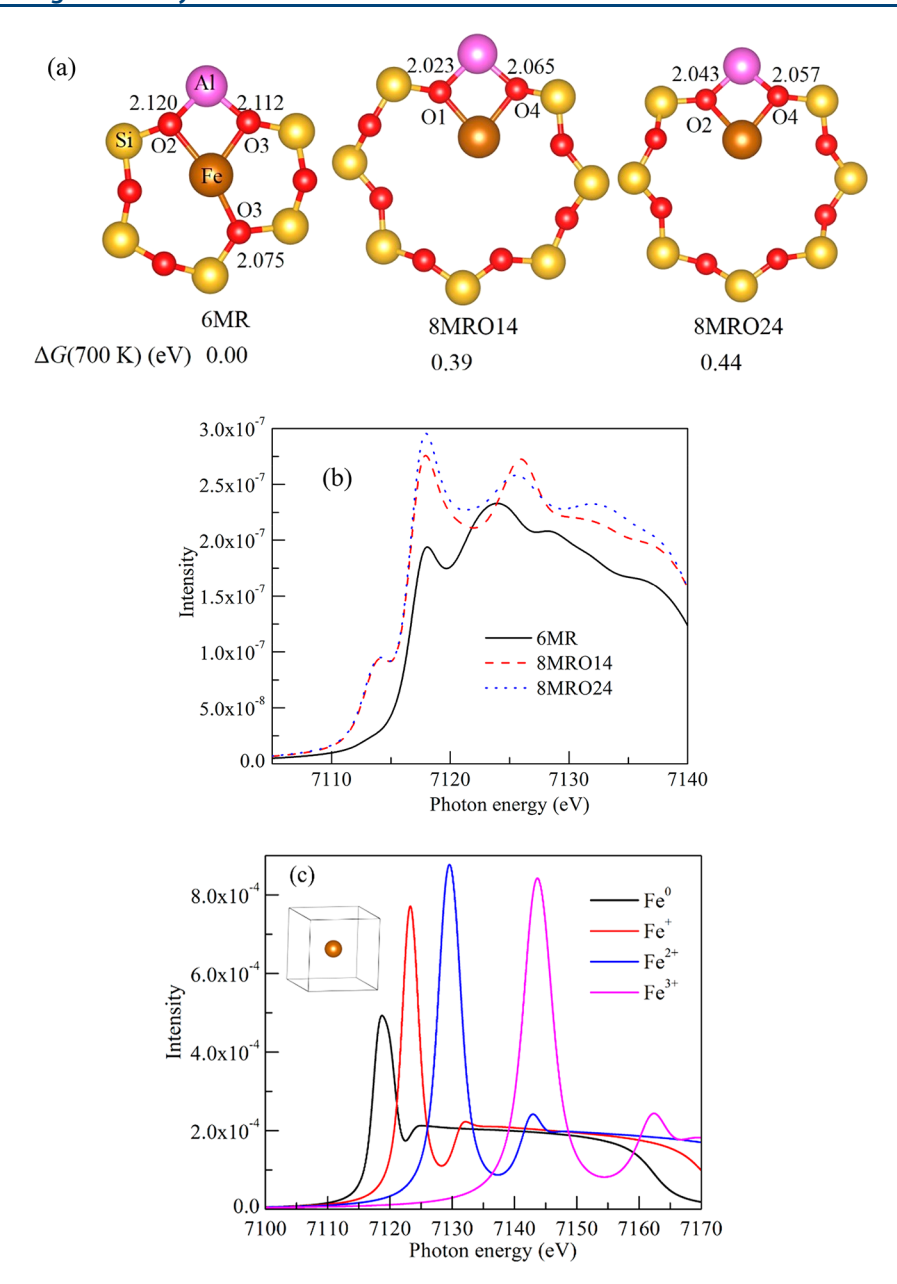


Figure 1. (a) Local structure of Fe⁺-SSZ-13 with Fe in 6MR, 8MRO14, and 8MRO24 sites. The distances between the Fe cation and the framework O anions in Å are listed in the figure. $\Delta G(700 \text{ K})$ is the Gibbs energy difference with respect to the Gibbs energy of the conformation with Fe in the 6MR site at 700 K. (b) Fe K-edge XANES of clean ZFe with Fe in the 6MR, 8MRO14, and 8MRO24 sites. (c) K-edge XANES of a Fe atom/cation in box with oxidation state of 0, +1, +2, and +3. The inset shows the structure of Fe atom/cation in a 10 Å × 11 Å × 12 Å box.

 NH_3) in Fe-SSZ-13 results in an improved high-temperature performance. This Fe/Cu-SSZ-13 co-catalyst was demonstrated to have high activity and excellent N_2 selectivity because of the synergistic effects between Cu and Fe.^{24,25} It was also reported that N_2O formation was significantly reduced upon the addition of Fe to a Cu-SSZ-13 sample.²⁵ Furthermore, trimetallic Ce-Fe-Cu-SSZ-13 was also reported to be a promising candidate for NH_3 -SCR technology because of the further synergistic effects of Cu, Fe, and Ce species.²⁶

The complementary advantages and synergistic effects of these types of catalysts attract more and more attention. However, much less is known about the basic chemistry of Fe-SSZ-13, such as the location of the Fe cation within the SSZ-13 framework and the location of the active site, as well as the underlying reaction mechanism. It is fundamentally important

to study the geometric and electronic structural characteristics of Fe-SSZ-13. Experimentally, the coordination chemistry of Fe cations in ion-exchanged Fe-SSZ-13 was characterized via infrared (IR) spectroscopy, using CO and NO probe molecules.²⁷ It was concluded that Fe²⁺ cations lying in the 6MR position can readily adsorb both CO and NO, but cannot form dinitrosyl or trinitrosyl complexes with NO. However, Fe²⁺ cations in the 8MR sites can form both dinitrosyl and trinitrosyl complexes. Gao et al. performed UV-vis, electron paramagnetic resonance (EPR), and Mossbauer spectroscopy, as well as temperature-programmed reduction and desorption experiments on Fe-SSZ-13 and concluded that the majority of the Fe species are extra-framework Fe³⁺ species ([Fe(OH)₂]⁺ and [HO-Fe-O-Fe-OH]²⁺).²⁸ Kovarik et al. studied the effect of hydrothermal aging on Fe-SSZ-13 using spectro-

scopic, microscopic, and kinetics methods and concluded that [HO-Fe-O-Fe-OH]²⁺ dimers are highly stable species.²⁹ A characteristic comparison study between Fe-SSZ-13 and Febeta also indicate that isolated and dinuclear Fe sites are primarily present in Fe-SSZ-13 while Fe-beta contains a high concentrations of oligomeric Fe_vO_v species.³⁰ In an effort to further understand the atomic structure and active sites of Fe-SSZ-13, we systematically study the location of the Fe cations within the SSZ-13 framework via DFT calculations in this work. Furthermore, we characterize the interaction of NO with Fe-SSZ-13 by comparing our computational results to the corresponding experimental IR spectra.

2. COMPUTATIONAL DETAILS

The DFT-based calculations of the energetics were performed using the Vienna Ab Initio Simulation Package (VASP).31,32 The projector augmented-wave (PAW)^{33,34} method was used to project the pseudo core-electron wave functions onto the atomic centers using the projection sets released prior to 2012.35 The generalized-gradient approximation (GGA), using the PW91 functional, 36 was employed for the treatment of the exchange-correlation effects. The total energy convergence threshold was set to 10⁻⁸ eV, and the geometries were considered to be fully relaxed when the forces were <0.01 eV/ Å. An energy cutoff of 400 eV was used for the determination of the plane-wave basis set. Γ-point sampling was used to sample the Brillouin zone in all our calculations.

As is well-known, the SSZ-13 zeolite belongs to the CHA structure, which consists of 4-membered rings (4MR), 6membered rings (6MR), and 8-membered rings (8MR) of Si and O atoms within the framework. A detailed structural model can be found in our previous work.8 In all calculations, a rhombohedral unit cell was employed. In order to obtain an accurate equilibrium volume, we followed a three-step procedure, which is detailed in the Supporting Information. For the purely siliceous chabazite, this procedure gives an equilibrium rhombohedral volume of 813.1 Å³, which has been reported in our previous work.8 In a rhombohedral unit cell, one Si atom can be replaced by one Al atom, which results in a one-electron deficit because the number of valence electrons in Si and Al are 4 and 3, respectively. An Fe cation can then be used to compensate for this electron deficiency. This zeolite is usually indicated as ZFe. Similarly, the replacement of two Si atoms by two Al atoms would also create cationic iron, indicated as Z₂Fe. The entire ZFe and Z₂Fe systems are charge neutral and the Fe cation has a formal oxidation state of Fe⁺ in the ZFe system and Fe²⁺ in the Z₂Fe system. The only calculations where the entire system is positively charged are those given in Figure 1c for Fe⁺, Fe²⁺, and Fe³⁺, where we considered an isolated Fe cation in a box. The calculated equilibrium volumes of ZFe and Z₂Fe are 810.5 and 828.8 Å³, respectively. As for the molecular adsorption calculations, the unit cells of the H2O conformation in ZFe and Z2Fe (H₂O ZFe and H₂O Z₂Fe) have equilibrium volumes of 820.9 and 818.3 Å³, respectively. It is found that the adsorption of H₂O increases the unit cell of ZFe while it decreases in Z₂Fe. The corresponding volume-energy plots are displayed in Figure S1 in the Supporting Information. Other adsorbates were studied using the lattice constants identified for the Fe-SSZ-13 conformations with H₂O. The adsorption energies (E_{ads}) were calculated by using the following equation:

$$E_{\rm ads} = E_{\rm tot} - E_{\rm ZFe} - E_{\rm mol} \tag{1}$$

where $E_{\rm tot}$, $E_{\rm ZFe}$, and $E_{\rm mol}$ are the total energies of ZFe in the presence of molecular adspecies, clean ZFe, and the isolated molecules in gas phase, respectively. In this work, we also discuss the Gibbs energy difference ΔG , which is the Gibbs energy difference for various configurations, with respect to a reference. The one with a ΔG value of 0.00 eV is the reference. We calculated the Gibbs energy by using the harmonic oscillator approach. In addition, to compare the relative stability of an Fe⁺ cation in ZFe and an Fe²⁺ cation in ZFeOH, we also constructed a phase diagram for the formation energy of ZFeO, H, conformations by using the following equations:

ZFe +
$$\left(\frac{y}{2}\right)$$
H₂O + $\left(\frac{2x-y}{4}\right)$ O₂ \rightarrow ZFeO_xH_y (2)

$$\Delta G_{\rm f} = G_{\rm ZFeO_xH_y} - G_{\rm ZFe} - \left(\frac{y}{2}\right)G_{\rm H_2O} - \left(\frac{2x - y}{4}\right)G_{\rm O_2}$$
(3)

The calculation of the theoretical K-edge XANES of Fe in Fe-SSZ-13 was performed using the CASTEP code,³⁷ as reported in our previous works.^{8,38} CASTEP uses a plane wave basis set and ultrasoft pseudopotentials. When the XANES calculations were performed, ultrasoft pseudopotentials were generated on the fly, 40 where one electron was removed from the 1s core level when performing the core-hole calculations. Furthermore, since the core-hole effect has a significant influence on the core level spectra, we took it into account in our calculations. 41 The Brillouin zone was sampled with a $(5 \times 5 \times 5)$ *k*-point grid. An energy cutoff of 550 eV was used for the determination of the plane-wave basis set, and a GGA-PBE³⁹ exchange-correlation functional was used in these XANES calculations. We also applied an energy broadening with an instrumental smearing of 0.6 eV (using the Gaussian method) and lifetime broadening of Fe with a value of 1.55 eV when calculating the XANES spectra.⁴⁰ For more details on the XANES calculations, we refer the reader to our previous work.8

3. RESULTS AND DISCUSSION

3.1. ZFe in the Presence (and in the Absence) of Adsorbates. Similar to what was found for the Cu cations in Cu-SSZ-13,8 there are three possible locations for the Fe cations, namely, the 6MR, 8MRO14, and 8MRO24 sites, as shown in Figure 1. Detailed information regarding the definition of such sites can be found in our previous work.8 We find that Fe in the 6MR site was 3-fold coordinated with O atoms, where Fe is bonded to an O2 oxygen atom with an Fe-O bond length of 2.120 Å and with two O3 atoms with Fe-O bond lengths of 2.112 and 2.075 Å, respectively. The Fe atoms in both 8MR sites are 2-fold coordinated with O atoms. In the 8MRO14 site, the Fe-O bond lengths are 2.023 and 2.065 Å, while they are 2.043 and 2.057 Å for Fe in the 8MRO24 site. Comparing the properties of Fe in different positions, we find that the 6MR site is the most thermodynamically favorable. The 8MRO14 and 8MRO24 sites are slightly less favorable, with Gibbs energy differences of 0.39 and 0.44 eV, respectively, at 700 K as compared to the 6MR site. The plots of the Gibbs energy, as a function of temperature, are shown in Figure S2 in the Supporting Information, as well as the H2O ZFe, OH ZFe, O ZFe, and NO ZFe conformations.

Figure 1b displays the theoretical Fe K-edge XANES of clean Fe⁺-SSZ-13 with Fe in the 6MR, 8MRO14, and 8MRO24 sites. There is a pre-edge in the Fe K-edge for both the 8MR sites, which is not present in the XANES when Fe is in the 6MR site and may be due to the different coordination number of Fe in the 6MR and 8MR sites. We also find that the intensity of the XANES for Fe in the 6MR site is weaker than that of Fe in the 8MR sites. The XANES edge position of Fe in the 6MR, 8MRO14, and 8MRO24 sites are 7116.79, 7116.68, and 7116.74 eV, respectively. These results indicate that the Fe cations in these different sites are in similar oxidation states. However, they have different feature peaks. As we previously reported for a Cu cation in SSZ-13, 42 the feature peaks are determined not only by oxidation state but also by local environment. To deconvolute the ligand environment effect with the oxidation state of the cation, we calculated the XANES of an isolated Fe atom/cation with a varying oxidation state. When comparing Figure 1b to Figure 1c, we see that the XANES features for the Fe⁺ cation in different coordination environments differ significantly to an isolated Fe⁺ cation, further demonstrating the importance of taking into account the ligand environment when interpreting the XANES features. Similar results for Cu atoms/cations are shown in Figure S3 in the Supporting Information.

The adsorption of atomic or molecular species on the active site of the ZFe conformation modifies the electronic and structural properties of the system, thus affecting its catalytic properties. Upon H_2O adsorption, it is found that the 8MR sites become more favorable than the 6MR site, where the Gibbs energy differences of the 8MRO14 and 8MRO24 sites, with respect to the 6MR site, are -0.26 and -0.21 eV, respectively (see Figure 2). The adsorption energies of H_2O on

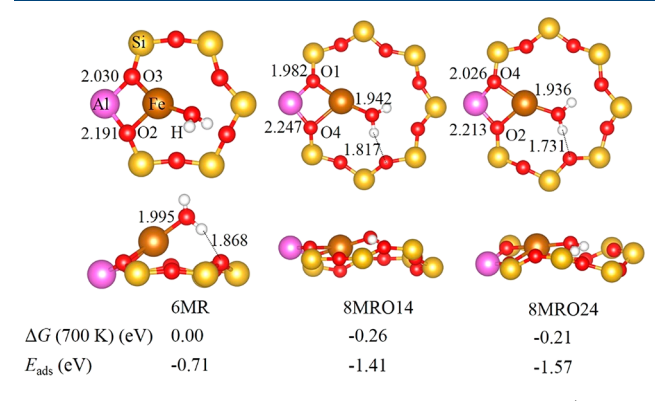


Figure 2. Local structures of H_2O adsorbed in an Fe⁺-SSZ-13 conformation with Fe in the 6MR, 8MRO14, and 8MRO24 sites. The distances between the Fe cation and the framework O anions in Å are indicated in the figure, as well as the Gibbs energy differences and the adsorption energies as defined in eq 1.

the Fe $^+$ cation in the 8MRO14 and the 8MRO24 sites are -1.41 and -1.57 eV, respectively, which are stronger than that of Fe in the 6MR (adsorption energy of -0.71 eV). For Fe in the 6MR, the adsorption of H₂O pulls the Fe cation out of the 6MR plane. Although the coordination number of Fe is still 3, the Fe cation is now bonded to two framework O atoms and the O atom in the H₂O molecule. For Fe in the 8MR sites, the adsorption of H₂O changes the coordination number of Fe to 3 as compared to 2 for the clean Fe $^+$ -SSZ-13 conformation. For all three sites of Fe, the H atom of the adsorbed H₂O molecule interacts weakly with the framework O atoms, where the nearest distances between H and framework O are 1.868, 1.817, and 1.731 Å for Fe in the 6MR, 8MRO14, and 8MRO24 sites, respectively.

In our previous work on Cu-SSZ-13,⁸ the adsorption of OH and O species increase the oxidation state of Cu. In this contribution, we adsorbed OH and O on ZFe with Fe in the 6MR, 8MRO14, and 8MRO24 sites. The local structures of OH and O adsorbed on ZFe are displayed in Figure 3. Upon

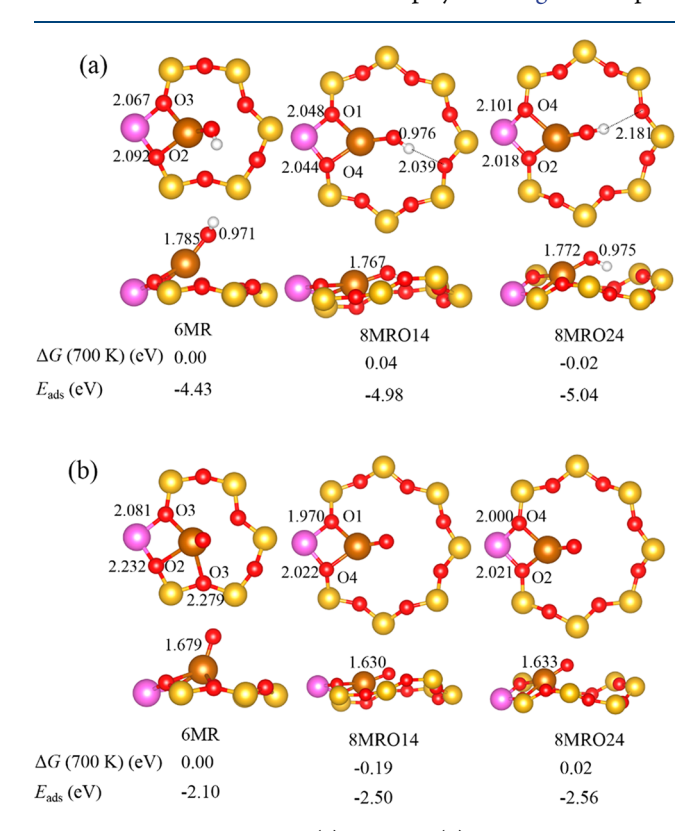


Figure 3. Local structures of (a) OH and (b) O adsorbed in a ZFe conformation with Fe in the 6MR, 8MRO14, and 8MRO24 sites. The distances between the Fe cation and the framework O anions are indicated in the figure, as well as the corresponding Gibbs energy differences and adsorption energies. The color coding for the other spheres and the given distances have the same meaning as in Figures 1 and 2.

OH and O adsorption, the energy differences between Fe in the 8MR and 6MR sites almost disappear, meaning that the thermodynamic stabilities of OH and O, when bonded to the different Fe sites, are almost identical within the ZFe conformation. The large negative adsorption energies of OH and O on Fe reflect their very strong interaction with Fe. We note that the adsorption energies for an O atom were calculated with respect to half the total energy of an $\rm O_2$ molecule.

As can be seen by examining Figure 4, the Fe K-edge positions in the simulated XANES vary significantly in the presence of OH and O as compared to that of the clean ZFe conformation. In the presence of OH and O, the Fe K-edge positions shift to higher-energy values of 0.97 and 1.97 eV, respectively. This shift quantitatively demonstrates that OH and O will oxidize Fe to higher oxidation states. In addition, the adsorption of OH and O results in a pre-edge peak at a photon energy of ~7113 eV in the Fe XANES K-edge.

The adsorption behavior of NO on ZFe is also important, not only because NO is one of the main reactants of the SCR reaction but also because NO can used as a probe molecule to study the coordination environment of metal-exchanged

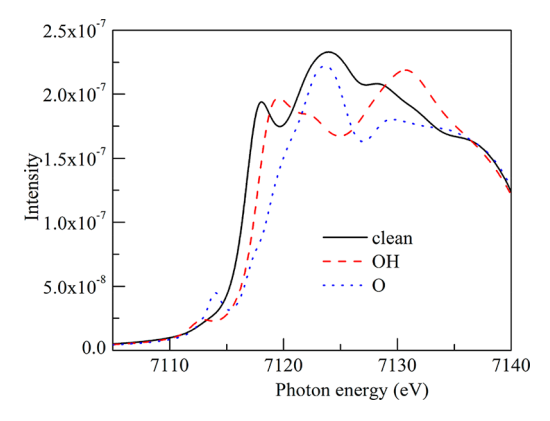


Figure 4. K-edge XANES of ZFe in the presence of OH and O, compared to a clean ZFe conformation with an Fe cation in a 6MR site

cations in different oxidation states.²⁷ The adsorption of NO results in the 8MR sites to become more favorable, similar to when water interacts with it. Furthermore, as can be seen in Figure 5, the NO stretching frequency decreases as compared

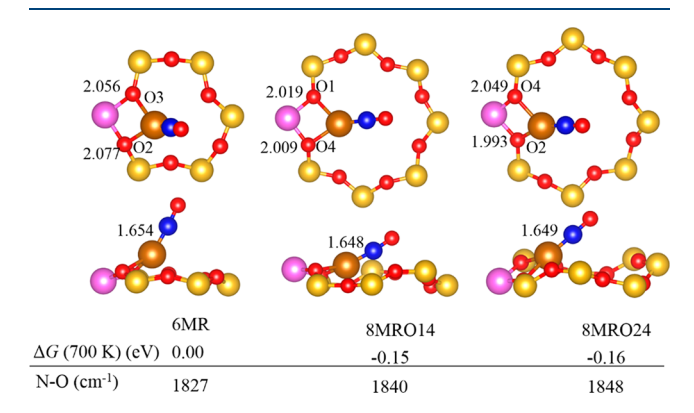


Figure 5. Local structures of NO adsorbed in the ZFe conformation with Fe in the 6MR, 8MRO14, and 8MRO24 sites. The distances between the Fe cation and the framework O anions in Å are indicated in the figure, as well as the Gibbs energy differences and N–O stretch frequencies.

to its gas-phase value of $1896~\rm cm^{-1}$, when it binds to an $\rm Fe^+$ cation. As a result, its N-O bond length also increases. Because of the instability of $\rm Fe^+$ cations, there are no IR peaks observed experimentally for $\rm Fe^+$ -NO in Fe-SSZ-13.

In Figure 6, we have constructed a phase diagram to compare the stability of the Fe $^+$ and Fe $^{2+}$ conformations that we have considered so far. We find that $\rm H_2O$ prefers to adsorb on a Fe $^+$ cation in the ZFe conformation for a wide range of temperatures. However, all Fe $^+$ conformations are less stable than the Fe $^{2+}$ conformations. Therefore, $\rm [Fe^{2+}(OH)]^+$ (low temperature) and $\rm [Fe^{2+}O]^+$ (high temperature) cations will be the more stable Fe cations in Fe-SSZ-13. In addition, the Fe cations always prefer the 8MR upon the adsorption of adspecies.

3.2. Z_2 Fe in the Presence (and the Absence) of Adsorbates. As mentioned above, Fe²⁺ cations can be generated by replacing two Si atoms with two Al atoms. We systematically studied the possible locations of an Fe²⁺ cation in Z_2 Fe, as well as possible relative positions of the two Al atoms, as shown in Figure S4 in the Supporting Information. From this analysis, similar to that observed for Cu²⁺ in SSZ-

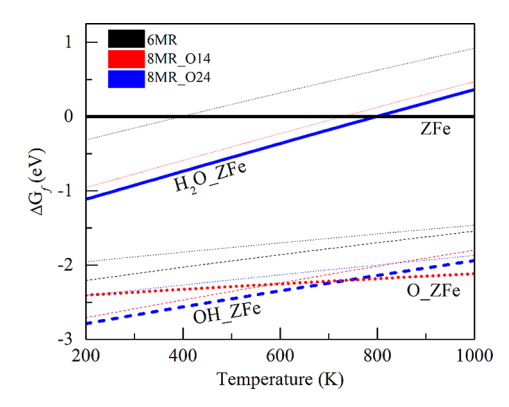


Figure 6. Phase diagram for ΔG_{θ} as a function of temperature at standard pressure of H_2O and O_2 , according to eq 3 for conformations of clean ZFe, H_2O _ZFe, OH_ZFe, and O_ZFe. We highlight the most favorable configuration for the Fe⁺ and Fe²⁺ conformations by thicker lines.

 $13,^{7,11,43}$ we conclude that the Fe²⁺ cation in the 6MR with an AlSiSiAl arrangement is the most favorable conformation, which is consistent with the work of Göltl et al. 44 However, a symmetrical Fe cation arrangement is reported to be the global minimum in the work of Göltl et al., 44 i.e., Fe bonded to the four activated O atoms, which differs from what is reported here. On the other hand, Göltl et al. used a PBE functional and a slightly different unit cell as compared to ours (we put the atomic positions of our Z₂Fe structure and the unit cell used in the Supporting Information). To determine which structure is the true global minimum, we reoptimized our Z₂Fe structure using the PBE functional, but did not change our unit-cell vectors. We then compared the total energy of that structure to the symmetrical one reported by Göltl et al., i.e., using the PBE functional and the unit-cell vectors as given in that contribution.⁴⁴ When comparing the energies of both structures, we find that the local arrangement as given in Figure 7b is slightly more favorable, by ~ 0.04 eV as compared

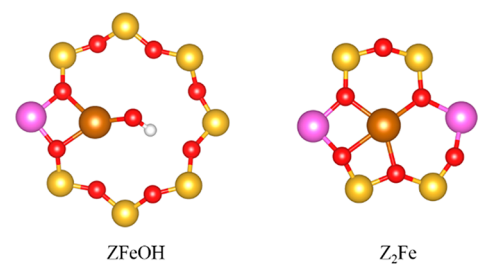


Figure 7. Most favorable conformations of the two types of Fe^{2+} cations in Fe-SSZ-13.

to the symmetrical one reported by Göltl et al. ⁴⁴ As such, the Z_2 Fe structure, as given in Figure 7, is the global minimum, but this conclusion depends sensitively on the choice of unit-cell vectors. We also note, as discussed in the previous section, that OH can oxidize an Fe⁺ cation to an Fe²⁺ cation and summarize the differences between these two types of Fe²⁺ cations in Figure 7.

The adsorption of NO and $\mathrm{NH_3}$ on an $\mathrm{Fe^{2+}}$ cation was also characterized from first principles. As such, we systemically tested several possible conformations of NO adsorbed on $\mathrm{Fe^{2+}}$ cations in ZFeOH and $\mathrm{Z_2Fe}$, which can be found in Figures S5 and S6 in the Supporting Information. Figure 8 shows the most favorable conformation for the adsorption of NO on $\mathrm{Fe^{2+}}$

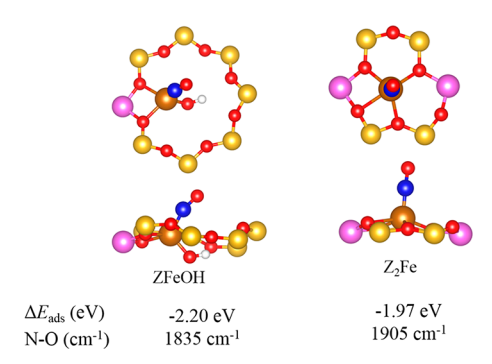


Figure 8. Adsorption of NO on Fe²⁺ cations in the ZFeOH and the Z_2 Fe conformations. The adsorption energies and the N-O stretch frequencies are given beneath the images in the figure.

cations in ZFeOH and Z_2Fe . It is found that these two types of Fe^{2+} cations have similar NO adsorption energies. However, the N–O stretch frequencies are very different on the two types of Fe^{2+} cations. As compared to the N–O stretch frequency in the gas phase of $1896~cm^{-1}$, the adsorption of NO in ZFeOH decreases its value to $1835~cm^{-1}$, while it increases its NO stretch frequency to $1905~cm^{-1}$ when it adsorbs on an Fe^{2+} cation within the Z_2Fe conformation. This result implies that OH greatly influences the NO stretch frequency. As for the interaction of NH₃ with Fe^{2+} cations, the most favorable conformations are shown in Figure 9. The other possible

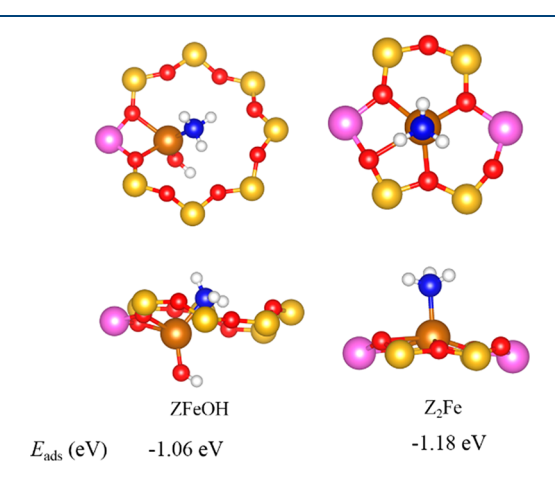


Figure 9. Adsorption of NH_3 on two different Fe^{2+} cations (the ZFeOH and Z_2Fe conformations). The adsorption energies are shown beneath the images in the figure.

adsorption conformations of NH_3 on Fe^{2+} cations can be found in Figures S7 and S8 in the Supporting Information. It is found that the adsorption energy of NH_3 is weaker than that of NO on Fe^{2+} cations. This means that the adsorption of NO can block the adsorption of NH_3 , since both participate in the SCR reaction.

3.3. [Fe³⁺(OH⁻)]²⁺ Species and NO Adsorption. More interestingly, it is experimentally reported that the major monomeric and dimeric Fe species are $[Fe(OH)_2]^+$ and $[HO-Fe-O-Fe-OH]^{2+}$ in Fe-SSZ-13.²⁸ This implies that OH plays a critical role in the redox chemistry of Fe cations. As a result, we characterized the relative stabilities of $[Fe^{3+}(OH^-)]^{2+}$ species in Fe-SSZ-13. We tested eight possible $[Fe^{3+}(OH^-)]^{2+}$ conformations in Fe-SSZ-13, which are shown in Figure S9 in the Supporting Information. The most favorable structure occurs in the 6MR with an AlSiSiAl

distribution. Upon the adsorption of NO, the stability of each conformation is displayed in Figure 10, with the corresponding

Relative Energies for Various Configurations Upon NO Adsorption On [Fe³⁺OH⁻]²⁺

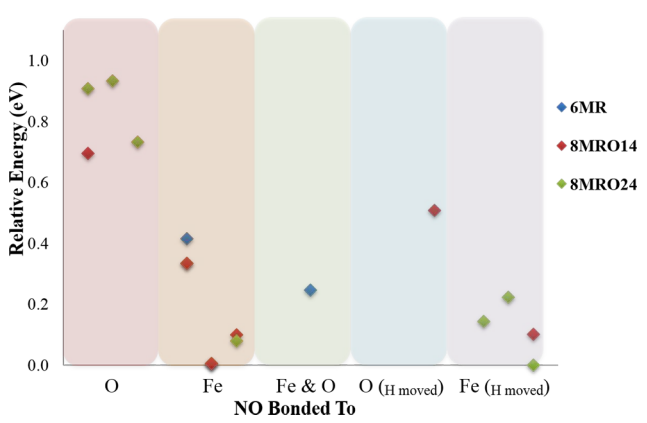


Figure 10. Relative energies (eV) of different optimized configurations of the $[Fe^{3+}(OH^-)]^{2+}$ species in the 6MR, 8MRO14, and 8MRO24 structures with different distributions of Al atoms.

structures given in Figure S10 in the Supporting Information. Unsurprisingly, the most favorable site for NO adsorption is when the Fe cation is within the 8MR. The adsorption of NO changes the relative favorability of the 6MR and 8MR structures, where the 8MR site is more favorable than the 6MR upon the adsorption of NO, while the 6MR is more favorable in the absence of NO. The most unfavorable configuration occurs when NO is adsorbed onto an O site in the 8MR.

3.4. Comparison between the Computational and Experimental Results of the NO IR Spectra. In order to understand the experimental IR results under different NO pressures, ²⁷ we studied the coadsorption of two and three NO molecules on Fe cations, as shown in Figure 11. Here, we

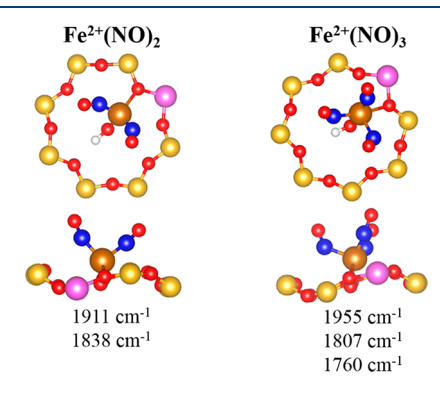


Figure 11. Structures of two and three NO molecules adsorbed on an Fe^{2+} cation in a ZFeOH conformation. The calculated NO frequencies are shown beneath the images in the figure.

mainly compare the NO stretch frequencies when NO is coadsorbed with an OH functional group that is bonded to an Fe²⁺ cation, since OH groups were experimentally determined to be present.²⁸ Note that the adsorption of a second NO molecule does not occur within the 6MR site. As such, we only consider the adsorption of multiple NO when the Fe cation is within an 8MR. When multiple NO molecules are adsorbed onto Fe, the vibrational frequencies are nowhere near identical,

since one can have symmetric and antisymmetric stretching modes. In Table 1, we compare the experimental and

Table 1. Comparison of Experimental NO Stretch Frequencies versus the Calculated Values Using DFT Calculations

	NO Stretch Frequencies (cm ⁻¹)	
	experiment	theory
Fe ²⁺ NO	1885	1835
		1905
2		
$Fe^{2+}(NO)_2$	1850	1911
	1771	1838
$Fe^{2+}(NO)_3$	1915	1955
	1812	1807
	1800	1760

computational results side by side. The experimental values for the NO stretch frequencies agree well with the DFT-calculated values, with the exception of $Fe^{2+}(NO)_2$. For $Fe^{2+}(NO)_2$, neither of the calculated values match closely to the experimentally determined band at 1771 cm⁻¹ which was assigned to the $Fe^{2+}(NO)_2$ species. Further investigation is needed in order to better explain this discrepancy.

4. CONCLUSION

In conclusion, we systematically studied the structural properties of Fe cations in Fe-SSZ-13 via DFT calculations. It is found that the most energetically favorable site for Fe occurs when it is located in the 6MR site while the 8MRO14 and 8MRO24 sites are less favorable with energy differences of 0.46 and 0.52 eV, respectively, with respect to the 6MR site. We find a pre-edge feature in the K-edge XANES of Fe in clean Fe⁺-SSZ-13 when Fe is in an 8MR site while there is no preedge peak when Fe is in a 6MR site, which is qualitatively similar to what we found for Cu-SSZ-13.8 Upon the adsorption of H₂O, OH, and O, the energy differences between Fe in the 8MR and 6MR sites almost disappear, which means that the thermodynamic stability of molecularly adsorbed Fe⁺-SSZ-13 is almost identical for Fe in different sites. Again, this result is similar to what we found on Cu-SSZ-13.8 We then examined both Fe^{2+} (as $[Fe(OH)]^+$) and Fe^{3+} (as $[Fe(OH)]^{2+}$) as possible active sites. Based on our results, the most energetically favorable site initially is the 6MR; however, with the addition of adsorbates, the 8MR will become more favorable. As such, our results show, for Fe2+, that the most stable configuration occurs within the 8MR where NO is coadsorbed on Fe with an OH ligand. As for the Fe³⁺ cation, the lowest energy configuration is achieved when NO adsorbs directly onto Fe within the 8MR without the interacting with the OH ligand. The properties of chemisorbed NO were studied by calculating their corresponding vibrational frequencies, which could be compared with experimental IR spectra. The experimental values for such frequencies agree well with the DFT-calculated values, except for $Fe^{2+}(NO)_2$.

Interestingly, the presence of OH groups seems to be important for Fe-SSZ-13. We also note that O binds much more strongly to an Fe⁺ cation than it did for a Cu cation. Furthermore, as shown in Figure S10 in the Supporting Information, we found several adsorption configurations where the O–H bond breaks and the H atoms binds to an adjacent O

atom within the zeolite framework. As such, a natural question here is whether the adsorbed OH groups that are bonded to the Fe cations could act as Brønsted acid sites, as was recently found to be the case in the condensed phase on Fe single-crystal surfaces. If this turns out to be the case, then the underlying SCR mechanism should be notably different to what was found on Cu-SSZ-13. 19,20

ASSOCIATED CONTENT

S Supporting Information

The Supporting Information is available free of charge on the ACS Publications website at DOI: 10.1021/acs.iecr.8b03643.

Volume—energy plots for the ZFe and Z_2Fe conformations, as well as the corresponding H_2O adsorbed conformations; possible locations of the Fe cation in Z_2Fe ; structures of NO and NH₃ adsorbed on Z_2Fe , ZFeOH; possible conformations of $[Fe^{3+}(OH^-)]^{2+}$ species in Fe-SSZ-13; structures of NO adsorbed on $[Fe^{3+}(OH^-)]^{2+}$ in Fe-SSZ-13 (PDF)

AUTHOR INFORMATION

Corresponding Author

*E-mail: js.mcewen@wsu.edu.

ORCID ®

Renqin Zhang: 0000-0002-4489-2050 Jean-Sabin McEwen: 0000-0003-0931-4869

Notes

The authors declare no competing financial interest.

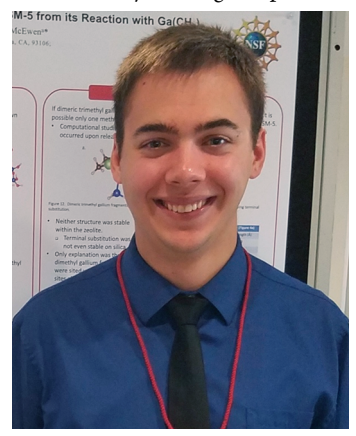
Biographies



Renqin Zhang received his Ph.D. in 2011 at Jilin University, China. He worked in Yonsei University for one year as a BK21 fellow. From 2012 to 2018, he was a postdoctoral research associate in Washington State University, where his research focused on computational catalysis for energy conversion and emission control. Now, he continues his research at The University of Texas at Austin.



Emily Anderst worked on reducing emissions in lean-burn engines an undergraduate within the McEwen research group in 2015. In 2016, she worked on the improvement of aftertreatment systems in diesel vehicles at PACCAR. She obtained her Bachelor's Degree in Chemical Engineering from Washington State University in the spring of 2017. She is currently working as a process engineer at Shell.



Kyle Groden obtained his Bachelor's Degree in Chemical Engineering from Washington State University in the spring of 2017. Following graduation, he immediately began pursuing a Ph.D. at Washington State University in Prof. Jean-Sabin McEwen's research group. His research has included investigation of Al site-pairing in medium-pore zeolites using organometallic probe molecules, as well as theoretical catalytic analysis of isolated precious metal atoms supported on thin-film oxides.



Jean-Sabin McEwen is an Associate Professor of the Voiland School of Chemical Engineering and Bioengineering at Washington State University and a Staff Scientist at the Pacific Northwest National Laboratory. He earned his B.Sc. in Physics at McGill University, Canada. He then went on to earn his M.Sc. and his Ph.D. in Physics

under the guidance of Hans Jürgen Kreuzer from Dalhousie University, Canada. He spent approximately two years as a postdoctoral fellow in Belgium at the Université Libre de Bruxelles in the group of Pierre Gaspard and three years in Belgium at the F.R.S.-FNRS as a Chargé de Recherches. He went on to obtain a position as a research assistant professor at the University of Notre Dame for two years in the group led by William F. Schneider. His expertise lies in the application of electronic structure calculations (density functional theory) and the development of multiscale kinetic models to problems in heterogeneous catalysis, electrocatalysis, and surface science. Dr. McEwen won the NSF CAREER award in 2017. He serves as the Secretary of the Pacific Coast Catalysis Society. He is also currently a member of the Early Career Advisory Board of ACS Catalysis.

ACKNOWLEDGMENTS

This invited contribution is part of the *I&EC Research* special issue for the 2018 Class of Influential Researchers. This work was supported by the National Science Foundation GOALI program, under Contract No. CBET-1258717. A portion of the computer time for the computational work was also performed using EMSL, a national scientific user facility sponsored by the Department of Energy's office of Biological and Environmental Research and located at Pacific Northwest National Laboratory (PNNL). PNNL is a multiprogram national laboratory operated for the United States Department of Energy (US DOE) by Battelle. This research also used resources from the Center for Institutional Research Computing at Washington State University. We finally also thank Dr. Janos Szanyi and Dr. Feng Gao for their useful suggestions and comments.

■ REFERENCES

- (1) Goralski, C. T.; Schneider, W. F. Analysis of the thermodynamic feasibility of NO_x decomposition catalysis to meet next generation vehicle NO_x emissions standards. *Appl. Catal., B* **2002**, 37, 263–277.
- (2) Deka, U.; Lezcano-Gonzalez, I.; Weckhuysen, B. M.; Beale, A. M. Local Environment and Nature of Cu Active Sites in Zeolite-Based Catalysts for the Selective Catalytic Reduction of NO_x. *ACS Catal.* **2013**, *3*, 413–427.
- (3) Matsumoto, S. I. Catalytic Reduction of Nitrogen Oxides in Automotive Exhaust Containing Excess Oxygen by NO_x Storage-Reduction Catalyst. *CATTECH* **2000**, *4*, 102–109.
- (4) Kwak, J. H.; Tonkyn, R. G.; Kim, D. H.; Szanyi, J.; Peden, C. H. F. Excellent activity and selectivity of Cu-SSZ-13 in the selective catalytic reduction of NO_x with NH₃. *J. Catal.* **2010**, 275, 187–190.
- (5) Beale, A. M.; Gao, F.; Lezcano-Gonzalez, I.; Peden, C. H. F.; Szanyi, J. Recent advances in automotive catalysis for NO_x emission control by small-pore microporous materials. *Chem. Soc. Rev.* **2015**, 44, 7371–7405.
- (6) Fickel, D. W.; D'Addio, E.; Lauterbach, J. A.; Lobo, R. F. The ammonia selective catalytic reduction activity of copper-exchanged small-pore zeolites. *Appl. Catal., B* **2011**, *102*, 441–448.
- (7) Zhang, R.; McEwen, J.-S.; Kollár, M.; Gao, F.; Wang, Y.; Szanyi, J.; Peden, C. H. F. NO Chemisorption on Cu/SSZ-13: A Comparative Study from Infrared Spectroscopy and DFT Calculations. ACS Catal. 2014, 4, 4093–4105.
- (8) Zhang, R.; Szanyi, J.; Gao, F.; McEwen, J.-S. The interaction of reactants, intermediates and products with Cu ions in Cu-SSZ-13 NH₃ SCR catalysts: an energetic and ab initio X-ray absorption modeling study. *Catal. Sci. Technol.* **2016**, *6*, 5812–5829.
- (9) Szanyi, J.; Kwak, J. H.; Zhu, H.; Peden, C. H. F. Characterization of Cu-SSZ-13 NH₃ SCR catalysts: an in situ FTIR study. *Phys. Chem. Chem. Phys.* **2013**, *15*, 2368–2380.

- (10) McEwen, J.-S.; Anggara, T.; Schneider, W. F.; Kispersky, V. F.; Miller, J. T.; Delgass, W. N.; Ribeiro, F. H. Integrated operando X-ray absorption and DFT characterization of Cu–SSZ-13 exchange sites during the selective catalytic reduction of NO_x with NH₃. *Catal. Today* **2012**, *184*, 129–144.
- (11) Deka, U.; Juhin, A.; Eilertsen, E. A.; Emerich, H.; Green, M. A.; Korhonen, S. T.; Weckhuysen, B. M.; Beale, A. M. Confirmation of Isolated Cu²⁺ Ions in SSZ-13 Zeolite as Active Sites in NH₃-Selective Catalytic Reduction. *J. Phys. Chem. C* **2012**, *116*, 4809–4818.
- (12) Bates, S. A.; Verma, A. A.; Paolucci, C.; Parekh, A. A.; Anggara, T.; Yezerets, A.; Schneider, W. F.; Miller, J. T.; Delgass, W. N.; Ribeiro, F. H. Identification of the active Cu site in standard selective catalytic reduction with ammonia on Cu-SSZ-13. *J. Catal.* **2014**, *312*, 87–97.
- (13) Kwak, J. H.; Varga, T.; Peden, C. H. F.; Gao, F.; Hanson, J. C.; Szanyi, J. Following the movement of Cu ions in a SSZ-13 zeolite during dehydration, reduction and adsorption: A combined in situ TP-XRD, XANES/DRIFTS study. *J. Catal.* **2014**, *314*, 83–93.
- (14) Paolucci, C.; Verma, A. A.; Bates, S. A.; Kispersky, V. F.; Miller, J. T.; Gounder, R.; Delgass, W. N.; Ribeiro, F. H.; Schneider, W. F. Isolation of the Copper Redox Steps in the Standard Selective Catalytic Reduction on Cu-SSZ-13. *Angew. Chem., Int. Ed.* **2014**, *53*, 11828–11833.
- (15) Borfecchia, E.; Lomachenko, K. A.; Giordanino, F.; Falsig, H.; Beato, P.; Soldatov, A. V.; Bordiga, S.; Lamberti, C. Revisiting the nature of Cu sites in the activated Cu-SSZ-13 catalyst for SCR reaction. *Chem. Sci.* **2015**, *6*, 548–563.
- (16) Gunter, T.; Carvalho, H. W. P.; Doronkin, D. E.; Sheppard, T.; Glatzel, P.; Atkins, A. J.; Rudolph, J.; Jacob, C. R.; Casapu, M.; Grunwaldt, J.-D. Structural snapshots of the SCR reaction mechanism on Cu-SSZ-13. *Chem. Commun.* **2015**, *51*, 9227–9230.
- (17) Lezcano-Gonzalez, I.; Wragg, D. S.; Slawinski, W. A.; Hemelsoet, K.; Van Yperen-De Deyne, A.; Waroquier, M.; Van Speybroeck, V.; Beale, A. M. Determination of the Nature of the Cu Coordination Complexes Formed in the Presence of NO and NH₃ within SSZ-13. *J. Phys. Chem. C* 2015, 119, 24393–24403.
- (18) Paolucci, C.; Parekh, A. A.; Khurana, I.; Di Iorio, J. R.; Li, H.; Albarracin Caballero, J. D.; Shih, A. J.; Anggara, T.; Delgass, W. N.; Miller, J. T.; Ribeiro, F. H.; Gounder, R.; Schneider, W. F. Catalysis in a Cage: Condition-Dependent Speciation and Dynamics of Exchanged Cu Cations in SSZ-13 Zeolites. *J. Am. Chem. Soc.* **2016**, 138, 6028–6048.
- (19) Gao, F.; Mei, D.; Wang, Y.; Szanyi, J.; Peden, C. H. F. Selective Catalytic Reduction over Cu/SSZ-13: Linking Homo- and Heterogeneous Catalysis. *J. Am. Chem. Soc.* **2017**, *139*, 4935–4942.
- (20) Paolucci, C.; Khurana, I.; Parekh, A. A.; Li, S.; Shih, A. J.; Li, H.; Di Iorio, J. R.; Albarracin-Caballero, J. D.; Yezerets, A.; Miller, J. T.; Delgass, W. N.; Ribeiro, F. H.; Schneider, W. F.; Gounder, R. Dynamic multinuclear sites formed by mobilized copper ions in NO_x selective catalytic reduction. *Science* **2017**, *357*, 898–903.
- (21) Brandenberger, S.; Kröcher, O.; Tissler, A.; Althoff, R. The State of the Art in Selective Catalytic Reduction of NO_x by Ammonia Using Metal-Exchanged Zeolite Catalysts. *Catal. Rev.: Sci. Eng.* **2008**, *50*, 492–531.
- (22) Gao, F.; Kollár, M.; Kukkadapu, R. K.; Washton, N. M.; Wang, Y.; Szanyi, J.; Peden, C. H. F. Fe/SSZ-13 as an NH₃-SCR catalyst: A reaction kinetics and FTIR/Mössbauer spectroscopic study. *Appl. Catal., B* **2015**, *164*, 407–419.
- (23) Gao, F.; Wang, Y.; Kollár, M.; Washton, N. M.; Szanyi, J.; Peden, C. H. F. A comparative kinetics study between Cu/SSZ-13 and Fe/SSZ-13 SCR catalysts. *Catal. Today* **2015**, *258*, 347–358.
- (24) Zhang, R.; Li, Y.; Zhen, T. Ammonia selective catalytic reduction of NO over Fe/Cu-SSZ-13. *RSC Adv.* **2014**, *4*, 52130–52139.
- (25) Wang, A.; Wang, Y.; Walter, E. D.; Washton, N. M.; Guo, Y.; Lu, G.; Peden, C. H. F.; Gao, F. NH₃-SCR on Cu, Fe and Cu⁺Fe exchanged beta and SSZ-13 catalysts: Hydrothermal aging and propylene poisoning effects. *Catal. Today* **2017**, DOI: 10.1016/j.cattod.2017.09.061.

- (26) Liu, X.; Li, Y.; Zhang, R. Ammonia selective catalytic reduction of NO over Ce-Fe/Cu-SSZ-13 catalysts. *RSC Adv.* **2015**, *5*, 85453–85459.
- (27) Szanyi, J.; Gao, F.; Kwak, J. H.; Kollar, M.; Wang, Y.; Peden, C. H. F. Characterization of Fe²⁺ ions in Fe,H/SSZ-13 zeolites: FTIR spectroscopy of CO and NO probe molecules. *Phys. Chem. Chem. Phys.* **2016**, *18*, 10473–10485.
- (28) Gao, F.; Zheng, Y.; Kukkadapu, R. K.; Wang, Y.; Walter, E. D.; Schwenzer, B.; Szanyi, J.; Peden, C. H. F. Iron Loading Effects in Fe/SSZ-13 NH₃-SCR Catalysts: Nature of the Fe Ions and Structure—Function Relationships. *ACS Catal.* **2016**, *6*, 2939—2954.
- (29) Kovarik, L.; Washton, N. M.; Kukkadapu, R.; Devaraj, A.; Wang, A.; Wang, Y.; Szanyi, J.; Peden, C. H. F.; Gao, F. Transformation of Active Sites in Fe/SSZ-13 SCR Catalysts during Hydrothermal Aging: A Spectroscopic, Microscopic, and Kinetics Study. ACS Catal. 2017, 7, 2458–2470.
- (30) Wang, A.; Wang, Y.; Walter, E. D.; Kukkadapu, R. K.; Guo, Y.; Lu, G.; Weber, R. S.; Wang, Y.; Peden, C. H. F.; Gao, F. Catalytic $\rm N_2O$ decomposition and reduction by NH $_3$ over Fe/Beta and Fe/SSZ-13 catalysts. *J. Catal.* **2018**, 358, 199–210.
- (31) Kresse, G.; Furthmüller, J. Efficient iterative schemes for ab initio total-energy calculations using a plane-wave basis set. *Phys. Rev. B: Condens. Matter Mater. Phys.* **1996**, *54*, 11169.
- (32) Kresse, G.; Hafner, J. Ab initio molecular dynamics for liquid metals. *Phys. Rev. B: Condens. Matter Mater. Phys.* **1993**, 47, 558.
- (33) Blöchl, P. E. Projector augmented-wave method. *Phys. Rev. B: Condens. Matter Mater. Phys.* **1994**, *50*, 17953.
- (34) Kresse, G.; Joubert, D. From ultrasoft pseudopotentials to the projector augmented-wave method. *Phys. Rev. B: Condens. Matter Mater. Phys.* **1999**, *59*, 1758–1775.
- (35) Lejaeghere, K.; Bihlmayer, G.; Björkman, T.; Blaha, P.; Blügel, S.; Blum, V.; Caliste, D.; Castelli, I. E.; Clark, S. J.; Dal Corso, A.; de Gironcoli, S.; Deutsch, T.; Dewhurst, J. K.; Di Marco, I.; Draxl, C.; Dułak, M.; Eriksson, O.; Flores-Livas, J. A.; Garrity, K. F.; Genovese, L.; Giannozzi, P.; Giantomassi, M.; Goedecker, S.; Gonze, X.; Grånäs, O.; Gross, E. K. U.; Gulans, A.; Gygi, F.; Hamann, D. R.; Hasnip, P. J.; Holzwarth, N. A. W.; Iuşan, D.; Jochym, D. B.; Jollet, F.; Jones, D.; Kresse, G.; Koepernik, K.; Küçükbenli, E.; Kvashnin, Y. O.; Locht, I. L. M.; Lubeck, S.; Marsman, M.; Marzari, N.; Nitzsche, U.; Nordström, L.; Ozaki, T.; Paulatto, L.; Pickard, C. J.; Poelmans, W.; Probert, M. I. J.; Refson, K.; Richter, M.; Rignanese, G.-M.; Saha, S.; Scheffler, M.; Schlipf, M.; Schwarz, K.; Sharma, S.; Tavazza, F.; Thunström, P.; Tkatchenko, A.; Torrent, M.; Vanderbilt, D.; van Setten, M. J.; Van Speybroeck, V.; Wills, J. M.; Yates, J. R.; Zhang, G.-X.; Cottenier, S. Reproducibility in density functional theory calculations of solids. Science 2016, 351, aad3000.
- (36) Perdew, J. P.; Wang, Y. Accurate and simple analytic representation of the electron-gas correlation energy. *Phys. Rev. B: Condens. Matter Mater. Phys.* **1992**, *45*, 13244.
- (37) Clark, S. J.; Segall, M. D.; Pickard, C. J.; Hasnip, P. J.; Probert, M. J.; Refson, K.; Payne, M. C. First principles methods using CASTEP. Z. Kristallogr. Cryst. Mater. 2005, 220, 567–570.
- (38) Zhang, R.; Helling, K.; McEwen, J.-S. Ab initio X-ray absorption modeling of Cu-SAPO-34: Characterization of Cu exchange sites under different conditions. *Catal. Today* **2016**, *267*, 28–40
- (39) Perdew, J. P.; Burke, K.; Ernzerhof, M. Generalized gradient approximation made simple. *Phys. Rev. Lett.* **1996**, *77*, 3865.
- (40) Gao, S.-P.; Pickard, C. J.; Perlov, A.; Milman, V. Core-level spectroscopy calculation and the plane wave pseudopotential method. *J. Phys.: Condens. Matter* **2009**, *21*, 104203.
- (41) Gao, S.-P.; Pickard, C. J.; Payne, M. C.; Zhu, J.; Yuan, J. Theory of core-hole effects in 1s core-level spectroscopy of the first-row elements. *Phys. Rev. B: Condens. Matter Mater. Phys.* **2008**, *77*, 115122.
- (42) Zhang, R.; McEwen, J.-S. Local Environment Sensitivity of the Cu K-Edge XANES Features in Cu-SSZ-13: Analysis from First-Principles. *J. Phys. Chem. Lett.* **2018**, *9*, 3035–3042.
- (43) Göltl, F.; Hafner, J. Structure and properties of metal-exchanged zeolites studied using gradient-corrected and hybrid

functionals. I. Structure and energetics. J. Chem. Phys. 2012, 136, 064501-17.

- (44) Göltl, F.; Müller, P.; Uchupalanun, P.; Sautet, P.; Hermans, I. Developing a Descriptor-Based Approach for CO and NO Adsorption Strength to Transition Metal Sites in Zeolites. *Chem. Mater.* **2017**, *29*, 6434–6444.
- (45) Hensley, A. J. R.; Wang, Y.; Mei, D.; McEwen, J.-S. Mechanistic Effects of Water on the Fe-Catalyzed Hydrodeoxygenation of Phenol. The Role of Brønsted Acid Sites. *ACS Catal.* **2018**, *8*, 2200–2208.